REVISED VERSION of paper that was originally published in the
Proceedings of the 17th International Ship Stability Workshop, 10-12 June 2019, Helsinki, Finland

Computational Fluid Dynamics Prediction of Hydrodynamic Derivatives for Maneuvering Models of a Fully-Appended Ship

Shawn Aram, *David Taylor Model Basin (NSWCCD)* shawn.aram@navy.mil

Kevin M. Silva, *David Taylor Model Basin (NSWCCD)* kevin.m.silva1@navy.mil

ABSTRACT

The utilization of Computational Fluid Dynamics (CFD) in the field of ship hydrodynamics is increasing. With the development of more robust and efficient solvers and growing computational resources at high-performance computing centers, more CFD is being utilized in everyday design. However, the computational burden still limits the efficiency of utilizing CFD for predicting long-running time-accurate seakeeping simulations in waves that are required to perform statistical analysis of extreme and rare ship motion events. The presented study builds upon previous work presented by Silva and Aram (2018) and calculates the hydrodynamic derivatives of the fully-appended Office of Naval Research Tumblehome (ONRTH). The hydrodynamic derivatives are then implemented within a maneuvering model and used to simulate a turning circle.

Keywords: *CFD, Maneuvering Models*

1. INTRODUCTION

CFD is increasingly being utilized in the field of ship hydrodynamics due to its ability to include a broader range of the physics involved in the ship-water interaction and is becoming a popular compliment and even alternative to traditional model testing. However, the computational cost of CFD is still its largest hindrance and it is currently impractical to simulate the long hours (1+ hours per condition) of ship motion that are typically required in dynamic stability assessments and the prediction of rare and extreme ship motion events. An effective and practical use of CFD is in the development of ship-specific inputs into maneuvering models that approximate the viscous contributions within other ship hydrodynamic simulations. The utilization of maneuvering models is typically heavily dependent on a series of experiments that are tailored to calculate hydrodynamic derivatives or coefficients that help describe the forces acting on the hull. Traditionally, these hydrodynamic derivatives are calculated with captive model tests or full-scale trials, but these require the physical construction of a model or ship and the depend on the availability and cost of facilities. CFD is an attractive alternative to these expensive tests due to the relatively straight-forward simulations required to calculate the hydrodynamic derivatives and the ability to easily change fluid and ship properties.

Maneuvering models have been utilized to assess a variety of aspects related to a ship's performance, but a particularly important area of implementation is in the prediction of extreme events. Simulations for the statistical analysis of extreme ship motion events are required to be computationally efficient but must include enough physical phenomena to make accurate and meaningful predictions. Leveraging CFD to tune the maneuvering models allows them to remain computationally efficient while including ship-specific hydrodynamic contributions.

This study builds upon the previous work of Silva and Aram (2018) presented at STAB2018 and calculates hydrodynamics derivatives for the fully-appended ONRTH, as well demonstrates the utilization of the

hydrodynamic derivatives within turning circle simulations. The CFD simulations are revisited and a more accurate prediction of hydrodynamic coefficients are obtained.

2. NUMERICAL METHODOLOGY

2.1 CFD Solver - NavyFOAM

A United States Navy in-house CFD software, NavyFOAM, in this study performs a series of Reynolds Averaged Navier-Stokes (RANS)-based simulations of the ONRTH model. NavyFOAM is a suite of CFD codes developed with a C++ based open-source continuum mechanics software called OpenFOAM®. OpenFOAM/NavyFOAM makes use of object-oriented programming techniques offered by C++ language that allow maximization of code re-use, adopt layered development, expedite building top-level applications, and make runtime-selection of numerical schemes, solution algorithms, physical models, and file I/O. NavyFOAM offers additional libraries in areas such as discretization schemes and physical models. Several top-level solvers for single- and multi-phase flows have also been added in NavyFOAM aiming at marine applications including underwater vehicles, surface ships, and propulsors (Gorski et al., 2014). Solvers have also been developed to replicate conditions experienced during captive model tests including static drift, rotating arm, and rotating arm at a drift angle. NavyFOAM has been validated for various ship hydrodynamics applications (Gorski et al., 2014, Kim et al., 2017, Aram and Field, 2016, Aram and Kim, 2017, Bhushan et al., 2018).

The continuity and momentum equations are the governing equations for the incompressible single-phase flow in NavyFOAM:

$$\nabla \cdot \mathbf{u} = 0 \tag{1}$$

$$\frac{\partial \mathbf{u}}{\partial t} + \nabla \cdot (\mathbf{u}\mathbf{u}) = \frac{1}{\rho} \nabla \cdot \{ - p\mathbf{I} + \boldsymbol{\tau} \} \tag{2}$$

where $\mathbf{u}$ is the fluid velocity, p is the fluid pressure, $\boldsymbol{\tau} = \mu_{eff} \left(\nabla \mathbf{u} + \nabla \mathbf{u}^T \right) - \frac{2}{3} \mathbf{I} \rho k$ is the viscous/turbulent stress with $\mu_{eff} = \mu + \mu_t$ the effective dynamic viscosity, and k turbulent kinetic energy.

A cell-centered finite-volume method based on a multi-dimensional linear reconstruction scheme is adopted to discretize the Navier-Stokes equations in NavyFOAM, that permits use of arbitrary polyhedral cells. The advection term in the momentum equation is discretized by the 2nd-order upwind scheme with skewness correction employed for the diffusion term. The continuity, momentum, and turbulence equations are solved implicitly in a segregated manner. The Wilcox's k-ω (Wilcox, 2008) model models the turbulence.

2.2 Maneuvering Model

A number of maneuvering models have been developed for hydrodynamic simulations of ships, but typically they are driven by a set of hydrodynamic derivatives or coefficients that describe the relationship between forces and moments to quantities like lateral and yaw velocity. Each implementation of a maneuvering model can vary how the terms are non-dimensionalized and utilized, so tailoring the calculation of the coefficients to the intended maneuvering model is important. The maneuvering model selected for this study is a simple model of horizontal motion:

$$(M + A)\ddot{\vec{X}} + F_I\left(\dot{\vec{X}}\right) + F_H\left(\dot{\vec{X}}\right) + F_{RP}\left(\dot{\vec{X}}\right) = 0 \tag{3}$$

where $\ddot{\vec{X}}$ and $\dot{\vec{X}}$ are the second and the first derivative of the state vector defined in the ship-fixed coordinate system:

$$\dot{\vec{X}} = \begin{pmatrix} u \\ v \\ r \end{pmatrix} \quad \ddot{\vec{X}} = \begin{pmatrix} \dot{u} \\ \dot{v} \\ \dot{r} \end{pmatrix} \tag{4}$$

where u is the surge speed, v is the sway speed, and r is the yaw rate. M in Equation (3) is a mass matrix:

$$M = \begin{pmatrix} m & 0 & 0 \\ 0 & m & m \cdot x_g \\ 0 & m \cdot x_g & I_z \end{pmatrix} \quad (5)$$

where m is the mass of a ship, x_g is the position of the center of gravity and I_z is the moment of inertia about the z axis.

A in Equation (3) is the added mass matrix:

$$A = \begin{pmatrix} -X_{\dot{u}} & 0 & 0 \\ 0 & -Y_{\dot{v}} & -Y_{\dot{r}} \\ 0 & -N_{\dot{v}} & -N_{\dot{r}} \end{pmatrix} \quad (6)$$

$F_I\left(\dot{\vec{X}}\right)$ is a vector-valued function expressing the inertial forces:

$$F_I\left(\dot{\vec{X}}\right) = F_{IL}(u,v,r) + F_{IN}(u,v,r) = m\begin{pmatrix} 0 \\ -uv \\ -x_g uv \end{pmatrix} + m\begin{pmatrix} vr + x_g v^2 \\ 0 \\ 0 \end{pmatrix} \quad (7)$$

where F_{IL} corresponds to the linear-only model, while F_{IN} describes the nonlinear correction. For a linear model, u is constant, as it is assumed that there is no speed loss on the turn, so the term F_{IL} is, in fact, linear.

$F_H\left(\dot{\vec{X}}\right)$ is a vector-valued function expressing the hydrodynamic forces on the hull:

$$F_H\left(\dot{\vec{X}}\right) = F_I(u,v,r) = -\begin{pmatrix} X_H \\ Y_H \\ N_H \end{pmatrix} \quad (8)$$

The hydrodynamic reaction forces (X_H and Y_H) and moment (N_H) are approximated with the hydrodynamic derivatives based on Taylor series expansion from Spyrou and Tigkas (2007) and originally formulated in Mikelis (1985):

$$X_H = X_{\dot{u}}\dot{u} - Y_{\dot{v}}vr - Y_{\dot{r}}r^2 + X_{vr}vr + R(u) \quad (9)$$

$$Y_H = Y_{\dot{v}}\dot{v} + Y_{\dot{r}}\dot{r} + Y_v vU + Y_r rU + Y_{vv}v|v| + Y_{vr}v|r| + Y_{rr}r|r| \quad (10)$$

$$N_H = N_{\dot{r}}\dot{r} + N_{\dot{v}}\dot{v} + N_r rU + N_v vU + N_{rr}r|r| + N_{rrv}\frac{r^2 v}{U} + N_{vvr}\frac{v^2 r}{U} + N_\phi \phi U^2 + N_{v\phi}v|\phi|U + N_{r\phi}r|\phi|U \quad (11)$$

where $R(u)$ is a resistance in calm water and U is the ship speed. $R(u)$, $(Y_v v + Y_r r)U$, and $(N_r r + N_v v)U$ are linear terms in Equation (9) - (11), and the rest are nonlinear corrections. $F_{RP}\left(\dot{\vec{X}}\right)$ in Equation (3) is a vector valued function for the rudder and propeller forces and moments.

The traditional methodology of generating the hydrodynamic derivatives is through a series of captive model tests that are designed to isolate the force and moment dependency of certain variables. Three of the most common captive model tests are the static drift, rotating arm, and rotating arm with drift. The static drift test is operated by setting the vessel at numerous drift angles relative to the flow and towing it with a constant forward resultant speed. Performing the towing in this manner allows for a relation between the sway speed, v and the forces and moments to be developed.

Another traditional captive model test is the rotating arm, where the vessel is fixed at a prescribed distance from a central point and is oriented perpendicular to the moment arm. The vessel is then rotated around the central point at a constant rate that corresponds to a tangential speed that is equivalent to the desired forward speed. The rotating arm test allows for a relationship between forces, moments and the yaw rate. A variation of the rotating arm test with drift determines the relationship between the joint dependence of forces and moments on both v and r. The rotating arm with drift test is performed similarly to the rotating arm except the vessel is set at a drift angle and not set perpendicular to the moment arm.

By performing the steady state simulations of static drift, rotating arm and rotating arm with drift conditions, all the terms containing the time derivatives of velocity vector are eliminated from Equation (3). This equation now only boasts terms like Y_v, Y_{vv} and N_v that come directly from the static drift cases, Y_r, Y_{rr}, N_r and N_{rr} that come from the rotating arm case, and Y_{vr}, N_{rrv} and N_{vvr} that come from the cross-dependence of v and r derived in the rotating arm with drift test.

3. PROBLEM DESCRIPTION AND SETUPS

The main objective of this study is to obtain the hydrodynamic derivatives of a hullform by performing a series of captive model CFD simulations and use the resultant coefficients to evaluate the maneuvering model.

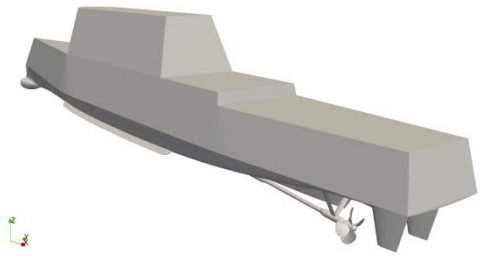

Figure 1 ONRTH model 5613.

Figure 1 shows the ONRTH model 5613, which is a fully appended 1/49 scale model equipped with a skeg, bilge keels, twin rudders, shafts and shaft brackets. Except the propeller geometry, the rest of appendages are considered in the current study. The main particulars of the model are presented in Table 1.

Table 1 Particulars of ONRTH model scale hull

Main Particulars	Model Scale
Displacement, Δ (kg)	72.6
Waterline Length, L (m)	3.147
Waterline Beam, B_{WL} (m)	0.384
Draft, T (m)	0.112
Wetted Surface Area, S (m^2)	1.5
L_{CB} (m aft of FP)	1.625
V_{CG} (m from keel)	0.156
Yaw Inertia (I_{yy}/L)	0.246
Propeller Diameter, D_p (m)	0.1066
Propeller Shaft Angle (deg)	5

Table 2 summarizes the CFD simulation conditions considered in this study, which includes the static drift and steady turn conditions. β and R are the drift angle and moment arm, respectively. All the simulations are performed to match the model scale Froude number of $Fr = 0.2$ and Reynolds Number of $Re = 3.48\times10^6$. The results of the entire run matrix are applied to generate all hydrodynamic derivatives used in simple model.

Table 2 Simulation conditions

Type	Case no.	β (deg)	R/L	r (rad/s)
Static Drift	1	0	∞	0
	2	2	∞	0
	3	4	∞	0
	4	6	∞	0
	5	8	∞	0
	6	10	∞	0
Steady Turn	7	0	2	0.176
	8	0	3	0.117
	9	0	4	0.088
	10	0	5	0.007
	11	0	10	0.035
	12	-2	2	0.176
	13	-6	2	0.176
	14	-2	3	0.117
	15	-6	3	0.117
	16	-2	4	0.088
	17	-6	4	0.088
	18	-2	5	0.007
	19	-6	5	0.007
	20	-2	10	0.035
	21	-6	10	0.035

The resultant hydrodynamic derivatives obtained from the CFD simulations are then employed within the potential flow simulation framework to predict ship stability and extreme events. Therefore, ignoring the free surface effects is necessary for calculating hydrodynamic derivatives. Removing the free surface effects warrants utilizing a single-phase scheme that only considers the static submerged geometry. This requirement indicates the advantage of numerical approach over the model tests for the presented maneuvering models. Only the underwater geometry shown in Figure 2 is considered in developing the computational domain.

HEXPRESS™, a commercial meshing software package from NUMECA generates non-conformal body-fitted full hexahedral unstructured meshes. Quadrilateral elements

predominantly construct the hull surface in combination with the local refinements to properly capture the sharp edges (see Figure 3). A refinement region around the hull as shown in Figure 4 increases the grid resolution in the vessel's wake region and allow for a smoother transition of cell sizing from the thin boundary layer cells with a y^+ (the average distance between the first cell center and vessel surface, in viscous unit) of 45 to the outer domain. The largest cell size (edge length) of the background grid is 0.75 m (~L/4) in all three directions. As depicted in Figure 5, the domain size is set to 16L, 12L, and 3.2L in the x, y, and z directions respectively, where x is positive aft, y is positive starboard, and z is positive up. The domain size is set to be large enough to accommodate all of the simulation conditions and resulted in a cell count of 2.86 million. The sensitivity of the computational results to the grid resolution is also examined by refining the grids on important regions, such as volumes around bow, stern, and wakes. The total number of elements of this refined grid is 7.13 million.

Figure 2 Underwater geometry of ONRTH.

Figure 3 Quadri-lateral surface grid elements on the ONRTH hull.

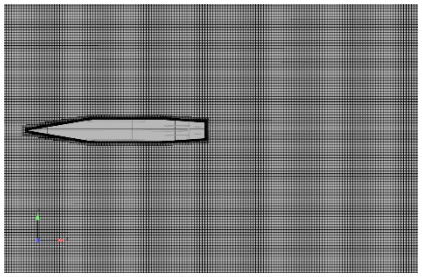

Figure 4 Depiction of the grid refinement regions around the ONRTH.

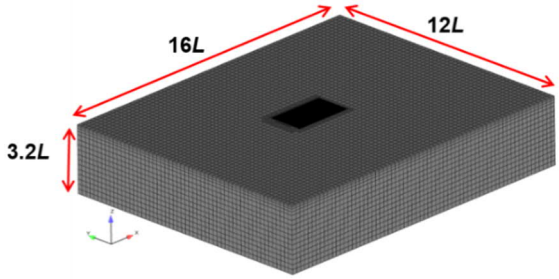

Figure 5 Isometric view of computational domain.

Since the simulations are only considering the underwater geometry, the free surface boundary utilizes a symmetry condition, also referred to as the "double-body" condition. Treating the free surface in this manner neglects the wavemaking effects and focuses on capturing the viscous contributions.

To simulate a captive model at a static drift condition, the x- and y-components of the velocity, u and v, on all boundaries of computational domain are set as illustrated in Figure 6 to reflect a drift angle of interest, β. Through this study, $\beta = \tan^{-1}(v/u)$.

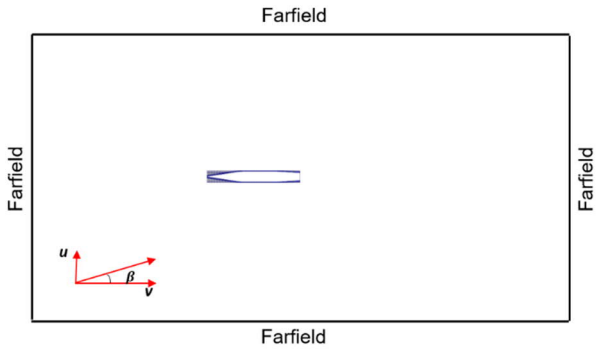

Figure 6 Illustration of velocity boundary condition for static drift cases.

The rotating arm captive model simulations are accomplished in NavyFOAM by adopting the single rotating frame (SRF) approach that solves the flow equations in a reference frame rotating at a constant rpm. Since this approach solves the equations for the absolute velocity instead of the relative velocity, a special type of boundary condition for velocity needs to be specified on the body surface that rotates with the SRF. The same computational domain as the

static drift case is used for this case. The captive rotating arm simulation with a drift angle could be achieved by rotating the computational domain by the drift angle around the center of buoyancy (CB), as illustrated in Figure 7.

To reduce the computational time, all the simulations are performed by the steady-state solvers in NavyFOAM without any time dependence in the momentum equations.

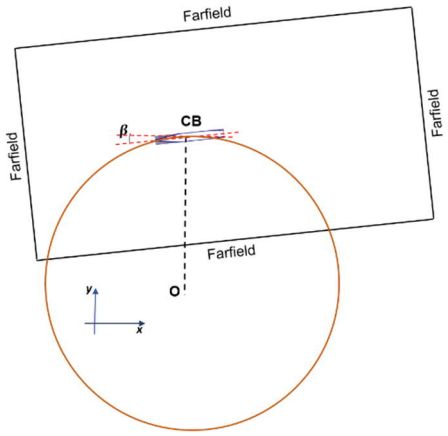

Figure 7 Computational domain for rotating arm simulation.

4. RESULTS AND DISCUSSION

Figure 8 compares the side force and yaw moment obtained from the two grid resolutions under the static drift condition. Y and N do not show any tangible difference in their results for the range of drift angles studied here. Based on this comparison, the original (coarse) grid is used for the rest of simulations.

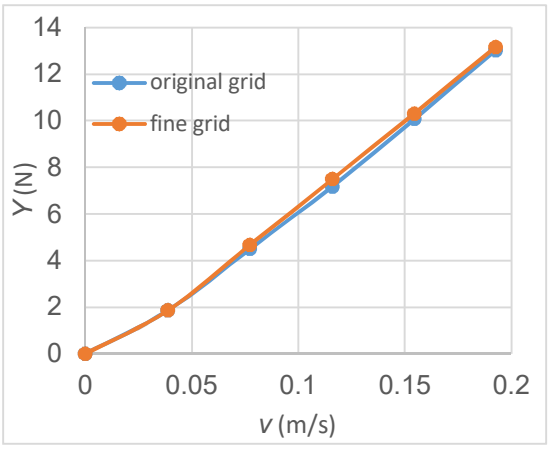

(a)

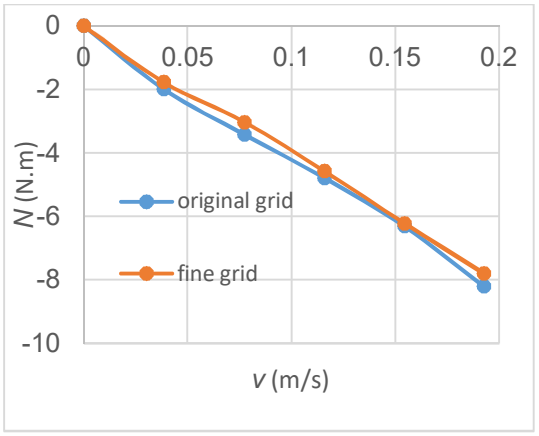

(b)

Figure 8 (a) Side force Y and (b) yaw moment N for static drift condition using two grid resolutions.

The iso-surface of non-dimensional Q criterion ($QL^2/U^2 = 8$) colored by the velocity magnitude for 0° and 10° static drift conditions is presented in Figure 9. A clear distinction is observed between the two cases, as large vortices extend from the bulbous bow and appendages for the higher drift angle. This is consistent with generation of large side force and yaw moment at the 10° drift angle.

Figure 10 shows the contours of absolute velocity magnitudes non-dimensionalized by the ship speed, $|U|/U_{FS}$ for the rotating arm condition at $R = 2L$ and 0° and 6° drift angles, as well as $R = 10L$ at 6° drift. A clear effect of drift angle in turn on the flow fields around the hull and in the wake of the ship is observed between Figure 10(a) and 10(b). As anticipated, changing the turning radius from $2L$ to $10L$ introduces significant effect on the ship wake.

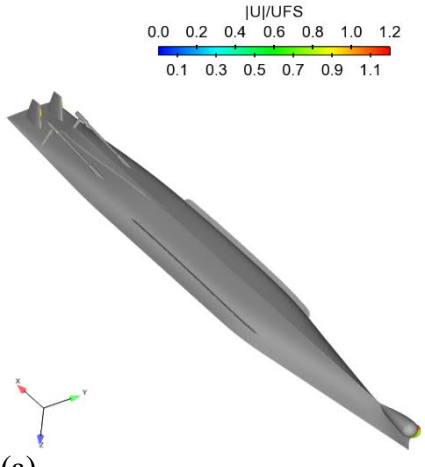

(a)

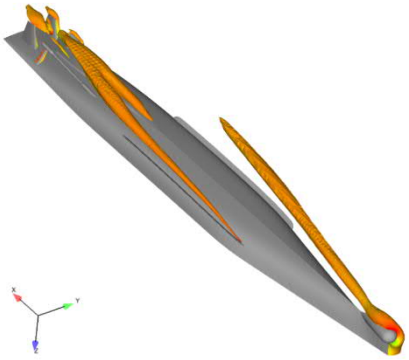

(b)

Figure 9 Iso-surface of non-dimensional Q criterion ($QL^2/U^2 = 8$) colored by the velocity magnitude for (a) 0° and (b) 10° at static drift.

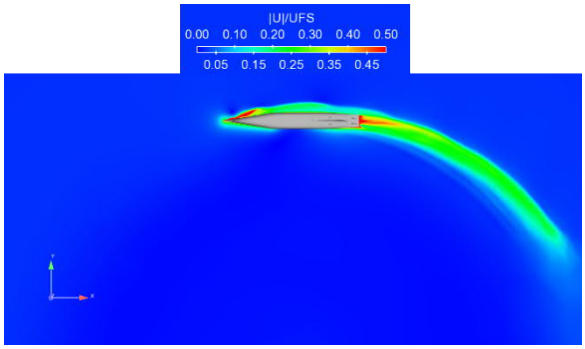

(a)

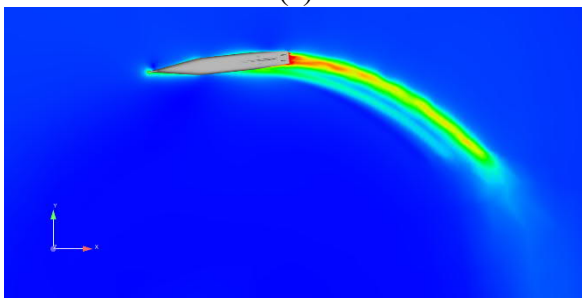

(b)

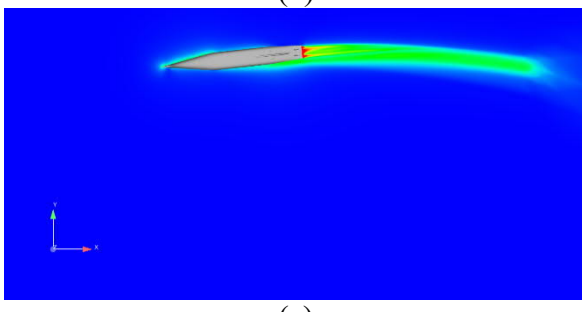

(c)

Figure 10 Comparison of velocity magnitude contours between (a) $2L$ at 0° drift, (b) $2L$ at 6° drift and (c) $10L$ at 6° drift.

Figure 11 plots the variation of the predicted side force and yaw moment with the v velocity under the static drift condition (red circles). The single-variable and multi-variable regression curves are also included in the figure. It is noticed that the coefficients of fitted polynomials for both regression methods are reasonably close. This indicates that the hydrodynamic coefficients Y_v, Y_{vv}, and N_v could be extracted accurately with six data points from static drift simulations in the current study.

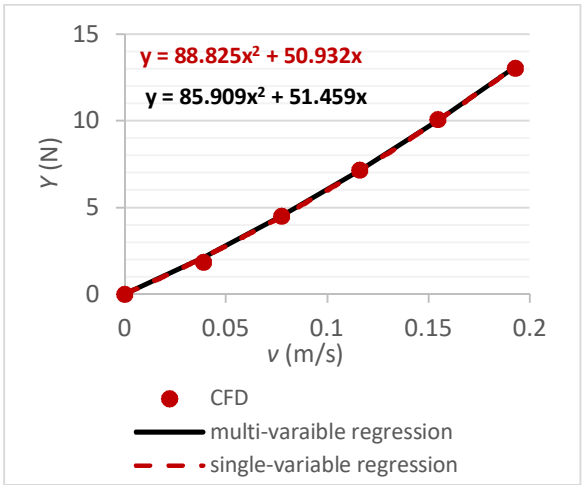

(a)

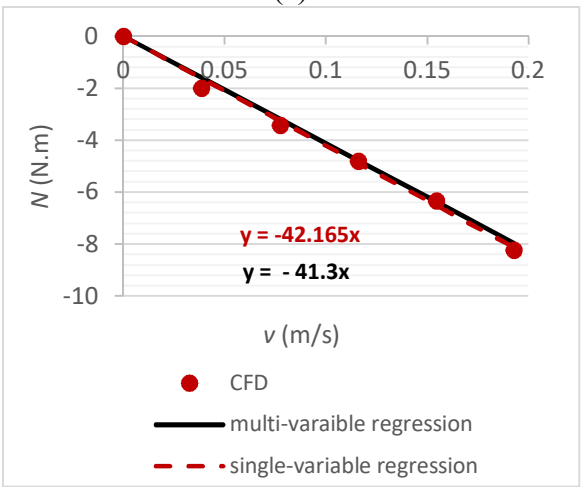

(b)

Figure 11 (a) Side force Y and (b) yaw moment N for static drift condition.

The CFD results of steady turn at zero drift versus the angular velocity along with the single- and multi-variable regression approach are shown in Figure 12. Although the polynomial coefficients of the fitted curves on the side force match closely between the two regressions, there is a significant difference on the second order term that represent N_{rr} between the two cases. This indicates that the five data points obtained from the steady turn simulations at zero drift are not sufficient to accurately extract N_{rr}.

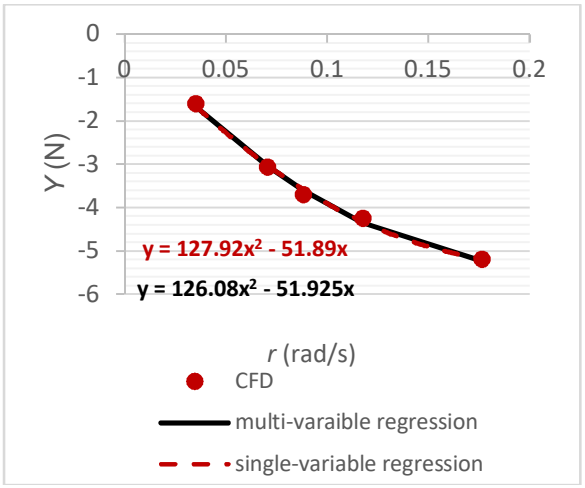

(a)

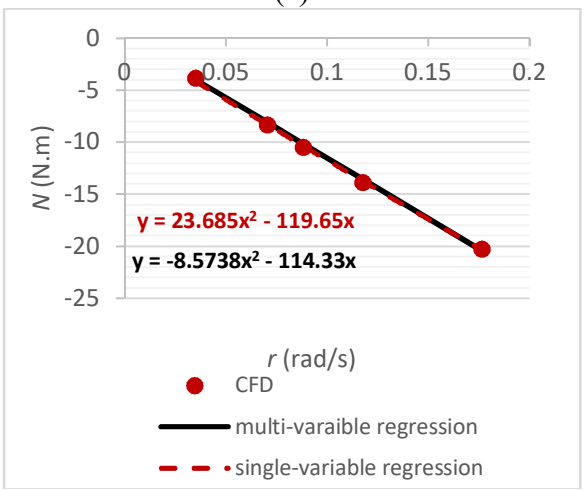

(b)

Figure 12 (a) Side force Y and (b) yaw moment N for static drift condition.

shows comparison of the hydrodynamic side force and yaw moment obtained from CFD under the rotating arm condition at three drift angles of 0º, -2º and -6º and selected angular velocities with those calculated from Equation (3). Close correlation between the CFD predictions and calculated derivatives are observed for both quantities, which is an indication of accuracy in the CFD results. Dependence of force and moment with r and v seen in these plots is also consistent with maneuvering behaviour of a ship under a steady turn.

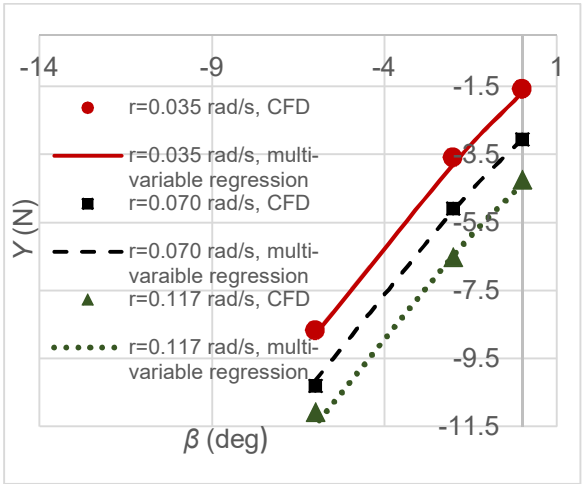

(a)

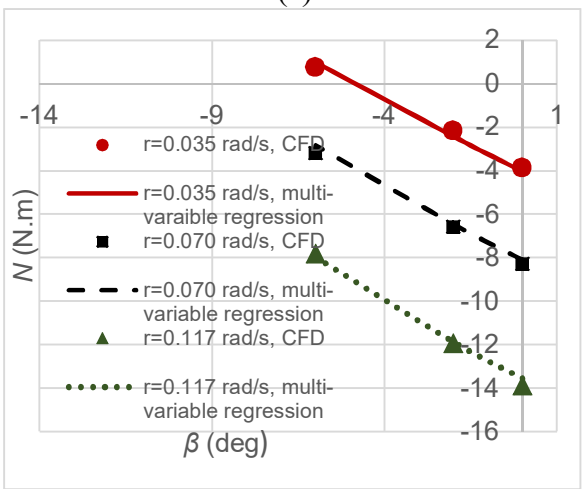

(b)

Figure 13. (a) Side force Y and (b) yaw moment N for rotating arm with selected angular velocities and drift angles.

The hydrodynamic coefficients obtained from the regression of the CFD results are summarized in Table 3. These results only utilized the underwater geometry of the ONRTH, therefore are applicable to any of the ONR Topside Series hullforms. The computational time to perform the simulations needed to develop the hydrodynamic derivatives presented in this study is around 80,000 CPU hours, relatively computationally inexpensive for CFD in naval applications. The proposed

methodology could be applied to develop larger matrices of testing conditions for numerous vessel configurations (e.g. with and without certain appendages). The analysis performed can also be used for additional post-processing analysis such as extracting sectional cross-flow drag characteristics as proposed in Hughes, et al. (2019).

Table 3 Predicted hydrodynamic derivatives

Hydrodynamic Derivatives	Non-dimensional values
X_{vr}	-0.0047271
Y_v	0.00903874
Y_{vv}	0.0175004
Y_r	-0.0029267
Y_{rr}	0.00254482
Y_{vr}	-0.00014481
N_r	-0.00214442
N_v	-0.00237815
N_{rr}	-0.00005419
N_{rrv}	0.00013022
N_{vvr}	0.0115384

The predicted hydrodynamic derivatives listed in Table 3 from model-scale CFD simulations are then employed to simulate a turning maneuver of the model-scale fully appended ONRTH. Figure 14 depicts the trajectory of ONRTH using the linear-only maneuvering model and simple model with non-linear corrections described in Section 2.2. The rudder angle deflected to a maximum angle of 35°. Considering the absence of the non-linear terms in the linear-only model, a reasonable trajectory of the ship is observed with about 2*L* in turning diameter. Adding the non-linear correction terms to the model leads to a more realistic behaviour of the ship with a slightly shorter transition distance and smaller turning radius (1.7*L*) due to the speed loss during turn.

Figure 15 shows the effect of *Fr* on the trajectory of the model-scaled ONRTH. As anticipated, increasing the *Fr* from 0.2 to 0.4 causes a slight increase in the turning diameter.

The ship trajectories presented here could indicate that the hydrodynamic derivatives are properly predicted by CFD.

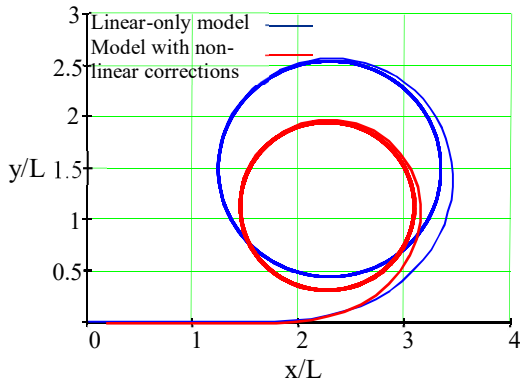

Figure 14. Sample trajectory of model-scale ONRTH using linear-only model and simple model with non-linear corrections: *Fr* = 0.2, maximum rudder angle 35°.

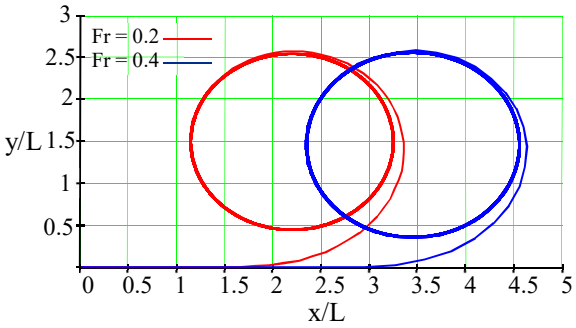

Figure 15. Sample trajectory obtained from simple model with non-linear corrections, computed in model-scale for *Fr* = 0.2 and 0.4, maximum rudder angle 35°.

5. CONCLUSIONS

The objective of this study was to showcase a simple procedure for a CFD-based prediction of hydrodynamic derivatives, so horizontal ship dynamics can be simulated with computational methods.

The described CFD calculations were completed for a model-scale fully appended hull and the results are significantly better compared to the previous attempt, performed for a bare hull.

However, including those appendages may not be the only reason for success. Performing CFD for fully appended hull may lead to double counting of the forces on control forces and how this double counting affects the results.

Another issue that became apparent is the influence of the multivariable regression. Some

criteria for goodness of regression could be useful for reliability of procedure.

In the future, the presented computational results will be validated against the available numerical and experimental data.

6. ACKNOWLEDMENTS

The presented work was sponsored by the Naval Surface Warfare Center Carderock Division (NSWCCD) Independent Applied Research (IAR) and In-house Laboratory Independent Research (ILIR) Programs under Dr. Jack Price.

Authors also would like to thank Ken Weems, Vadim Belenky, and Kostas Spyrou for their help with the maneuvering model.

7. REFERENCES

Aram, S., and Field, P. L., 2016, "CFD-Based Maneuvering Prediction of a Trimaran with Two Side Hull Configurations in Calm Water," SNAME Maritime Convention, Bellevue, Washington, USA.

Aram, S., and Kim, S. E., 2017, "A Numerical Study of Added Resistance, Speed Loss and Added Power of a Surface Ship in Regular Head Waves Using Coupled URANS and Rigid-Body Motion Equations," VII International Conference on Computational Methods in Marine Engineering, MARINE 2017, Nantes, France.

Bhushan, S., Yoon, H., Stern, F., Guilmineau, E., Visonneau, M., Toxopeus, S., Simonsen, C., Aram, S., Kim, S. E., and Grigoropoulos, G., 2018, "Assessment of CFD for Surface Combatant 5415 at Straight Ahead and Static Drift $\beta = 20^{o}$," Journal of Fluids Engineering, doi:10.1115/1.4041229.

Gorski, J., Kim, S. E., Aram, S., Rhee, B., and Shan, H., 2014, "Development of a CFD Framework for Prognoses of Resistance, Powering, Maneuvering, and Seakeeping of Surface Ships," Proceedings of 30th Symposium of Naval Hydrodynamics, Tasmania, Australia.

Hughes, M. J., Kopp, P. J., and Miller, R. W., 2019, "Modelling of Hull Lift and Cross Flow Drag Forces in Large Waves in a Computationally Efficient Dynamic Stability Prediction Tool," Chapter 5 of Contemporary Ideas on Ship Stability. Risk of Capsizing, Belenky, V., Spyrou, K., van Walree F., Neves, M. A. S., and Umeda, N. editors., Springer, ISBN 978-3-030-00514-6., pp 77-90.

Kim, S. E., Shan, H., Miller, R., Rhee, B., Vargas, A., Aram, S., and Gorski, J., 2017, "A Scalable and Extensible Computational Fluid Dynamics Software Framework for Ship Hydrodynamics Applications: NavyFOAM," Computing in Science & Engineering, Vol. 19, No. 6, pp. 33-39.

Mikelis, N., 1985, "A Procedure for the Prediction of Ship Manoeuvring Response for Initial Design," Proceedings of International Conference of Shipyard Operation and Ship Design, ICCAS, Banda, P., and Kuo, C., Elsevier Publishers B. V., North Holland.

Silva, K. M., and Aram, S., "Generation of Hydrodynamic Derivatives for ONR Topside Series Using Computational Fluid Dynamics," Proceeding of the 13th International Conference on the Stability of Ships and Ocean Vehicles, STAB2018, Kobe, Japan.

Spyrou, K. J., and Tigkas, I., 2007, "Dynamics of a ship steering win wind revisited," Journal of Ship Research, Vol. 51, No. 2, pp. 160-173.

Wilcox, D. C., 2008, "Formulation of the K-Omega Turbulence Model Revisited," AIAA Journal, Vol. 46, No. 11, pp. 2823-2838.